Journal of Power Sources 196 (2011) 1948–1954

Contents lists available at ScienceDirect

Journal of Power Sources

journal homepage: www.elsevier.com/locate/jpowsour

Voltage loss and fluctuation in proton exchange membrane fuel cells: The role of cathode channel plurality and air stoichiometric ratio

Nicholas S. Siefert, Shawn Litster*

Dept. of Mechanical Engineering, Carnegie Mellon University, Scaife Hall 323, 5000 Forbes Ave, Pittsburgh, PA 15213, USA

ARTICLE INFO

Article history:
Received 20 August 2010
Received in revised form 5 October 2010
Accepted 6 October 2010
Available online 14 October 2010

Keywords:
Proton exchange membrane fuel cell
Two-phase flow
Flooding
Instability
Microchannel
Water management

ABSTRACT

Water management is a critical issue in the development of proton exchange membrane (PEM) fuel cells with robust operation. Liquid water can accumulate and flood the gas delivery microchannels and the porous electrodes within PEM fuel cells and deteriorate performance. Since the liquid distribution fluctuates in time for two-phase flow, the rate of oxygen transport to the cathode catalyst layer also fluctuates, resulting in unstable power density and efficiency. This paper reports experimental data on the mean voltage loss and the voltage fluctuations during constant current operation as a function of both the number of parallel microchannels and the air flow rate stoichiometric ratio. We define channel plurality as a flow field design parameter to describe the number of channels per unit of active area. The voltage loss was found to scale proportionally to channel plurality divided by the air stoichiometric ratio. The amplitude of the voltage fluctuations was found to be linearly proportional to channel plurality and inversely proportional to the air stoichiometric ratio squared. By analyzing pressure drop data and power spectra, we conclude that the voltage fluctuations are well-correlated with two-phase flow instabilities in the cathode's parallel microchannels. Finally, a scaling analysis is presented for generalizing the results for fuel cells having different active area and channel cross-section.

1. Introduction

Proton exchange membrane (PEM) fuel cells are being developed for commercial applications in the areas of transportation, back-up power, and portable power. One of the main advantages of hydrogen fuel cell power generation compared with internal combustion power generation is the negligible tailpipe emission of pollutants, such as SO*x*, NO*x*, particulates and greenhouse gases [1]. Two remaining problems for the development of PEM fuel cells include the cost of the catalyst, and the cost and parasitic load of air delivery and water management components [2]. The costs and system-level power losses associated with air delivery are often increased by the need for high flow rates and pressure drops to drive liquid water out of the microchannels.

One goal in the development of PEM fuel cells for back-up power applications is to minimize the cost, size, and weight of the equipment required to flow air through the microchannels. This goal can be accomplished by operating at atmospheric pressure with low flow rates, so as to minimize the size and cost of air fans/blowers. This requires a flow field with a low pressure drop and that is robust to channel flooding. There are three main types of flow fields for feeding gases to the electrodes: serpentine, parallel, and interdigitated. A pure serpentine flow field consists of one channel that winds its way across the cathode electrode surface. Since there is only one channel, serpentine channels are very effective at removing liquid because of the high gas velocity. However, the pressure drop across the channel can be extremely large compared to the case when the cathode is covered by channels in parallel. The trade-off between serpentine and parallel flow fields is that the lower flow velocity (for a given total air flow rate) with parallel channels can cause liquid water to accumulate, resulting in plug flow or complete channel blockage and catastrophic voltage loss. Given this trade-off, flow fields with a large number of serpentine channels in parallel are common. The goal is to have as many channels in parallel as possible without introducing unmanageable channel flooding.

Another aspect driving the development of flow fields with more channels in parallel is the desire to reduce the depth of the channel without increasing the hydraulic resistance of the channel array. The motivation for shallower channels is to reduce plate thickness for greater volumetric power density and to reduce the material stresses and issues when fabricating stamped metal bipolar plates. Since at constant flow rate the single-phase flow pressure drop, Δp, scales with the inverse of the hydraulic diameter, D_h, to the 4th power, $\Delta p \propto 1/D_h^4$, it is necessary to use many channels in parallel to reduce the pressure drop for a given total flow rate.

* Corresponding author. Tel.: +1 412 268 3050; fax: +1 412 268 3348.
E-mail address: litster@andrew.cmu.edu (S. Litster).

0378-7753/$ – see front matter © 2010 Elsevier B.V. All rights reserved.
doi:10.1016/j.jpowsour.2010.10.026

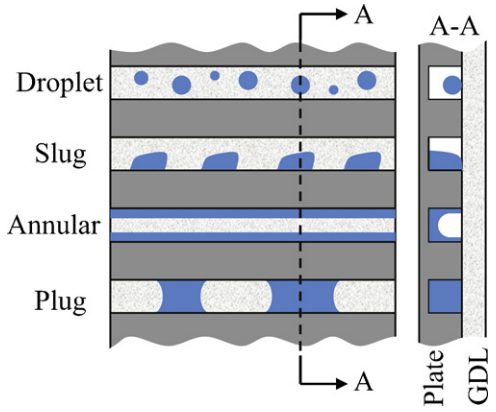

Fig. 1. Common two-phase flow regimes in PEMFC micro-channels. The flow is depicted for a hydrophobic GDL and a hydrophilic plate.

Increasing the number of channels in parallel reduces the pressure drop by lowering the average velocity in each channel and shortening the length of each channel. Thus, the single-phase pressure drop scales inversely with the square of the number of channels, $\Delta p_2/\Delta p_1 \cong (N_1/N_2)^2$.

Reviews of water flooding issues in PEM fuel cells have been conducted by Anderson et al. [3], Li et al. [4], and Minor et al. [5]. The topic of water droplet dynamics in fuel cell microchannels has been studied by many research groups [6–12]. In their recent study, Lu et al. [10] measured the fluctuations in the pressure drop across PEM fuel cell microchannels at a range of different values of u_l and u_g, and have related the amplitude of the pressure fluctuations to the different types of flow: mist < film (annular) < slug. Fig. 1 illustrates these common two-phase flow regimes in the microchannels of PEM fuel cells. Often, flow maps are presented to characterize the two-phase flow regime in microchannels as functions of the liquid and gas superficial velocities, u_l and u_g, which are the volumetric flow rates of liquid and gases divided by the total cross-sectional area of the channels. For example, Zhang et al. [12] performed *ex situ* experiments to evaluate the flow regimes in microchannels under conditions consistent with PEM fuel cell operation. Hussaini and Wang [13] performed *in situ* characterization of the flow regimes under different conditions in an operating PEM fuel cell with a transport plate for visualization.

One important gap in the understanding of PEM fuel cell water management is the scaling of the voltage loss and voltage fluctuations versus the number of parallel channels. So far, most experiments have been conducted using a single choice for the number of parallel microchannels. This paper presents the analysis of data collected using four different flow fields with 4, 8, 15 and 25 parallel microchannels. In this paper, we use the term 'channel plurality' to characterize the degree to which a channel configuration is serpentine-like or parallel-like. Channel plurality, χ, is defined as the number of independent channels, N, per unit area of active area, A, $\chi = N/A$. Thus, the values of channel plurality studied are 0.8, 1.6, 3, and 5 cm^{-2}. The channel plurality of the cathode flow fields recently studied by General Motors is 0.455 cm^{-2} [14]. In the Discussion section, we non-dimensionalize the channel plurality with the channel cross-sectional area according to the definitions of u_g and u_l. A small value of channel plurality implies a serpentine-like arrangement and a large value implies parallel-like channels. Small values of channel plurality are also obtained with a low number of very long channels (i.e., a straightened serpentine flow field).

An important feature of the present study is the design of the flow fields to carefully separate the effects of channel plurality. The key design features are the different active area aspect ratios for different numbers of channels, which allows the number of channels to change without the spurious effects of introducing bends into the channel layouts. We also designed the flow fields with large diameter header channels having a long flow development length to minimize their influence on the results and increase the microchannels' relative contribution to the measurements. We investigate the effect of channel plurality by evaluating the voltage loss and fluctuation scaling, and also by analyzing the power spectrums of fuel cell voltage versus frequency and the correlation with pressure drop measurements.

2. Experimental

Four different custom-made graphite cathode plates were constructed having 4, 8, 15 and 25 straight, parallel channels. Fig. 2 shows images of the four plates. The length of the parallel channels was chosen so that the total electrode area (the active area), which the parallel channels covered, was constant at 5 cm^2. In other words, the aspect ratio of the electrode was altered depending on the number of channels. Each channel was 1 mm in width and 0.5 mm in depth, and the rib width was 1 mm. The headers were designed so that the pressure drop along the headers was significantly less than the pressure drop through the channels, which should provide equal flow through each parallel channel in single phase flow conditions. The headers, before and after the parallel channels, were 8 mm in width and 4 mm in depth. Thus, the header channels are large enough that gravity can be used to direct the water in preferential directions. The header channels also featured a sufficiently long development length before the channels to ensure the flow in the header was fully developed and to further minimize channel flow variation. The microchannels were orientated such that the flow through the microchannels was in the same direction as the force of gravity, and therefore, the flow through the headers was perpendicular to the force of gravity. In the outlet header, the force of gravity pulls droplets away from the channel/outlet header interface, further reducing the effect of the header channels on the results.

The membrane electrode assembly (MEA) featured a 25 μm thick Nafion® membrane coated with cathode and anode catalyst layers (MEA 1017, Ion Power Inc., New Castle, DE). The gas diffusion layers (GDLs) were SGL Carbon 10 BB – Gas Diffusion Media (Ion Power Inc., New Castle, DE). Single-sided adhesive Teflon®-coated fiber glass gaskets (McMaster-Carr, Atlanta, GA) sealed the GDL perimeter and defined the 5 cm^2 active area within the 25 cm^2 MEA. A new MEA was prepared for each flow field plate tested in the commercial 50 cm^2 single cell hardware (Fuel Cell Technologies Inc., Albuquerque, NM). The anode flow field was the original 50 cm^2 4-channel serpentine flow field plate from the fuel cell hardware. Pressure sensitive paper (Sensor Products, Inc., Madison, NJ) was used to ensure that the 5 cm^2 active area was properly compressed in this novel arrangement. In addition, preliminary experiments were done to ensure the active area was properly masked and the area-specific current–voltage characteristics of the MEA were maintained.

All experiments were conducted on a commercial fuel cell test station (Fuel Cell Test Stand 850e, Scribner Associates, Southern Pines, NC). We set an operating pressure of 1 atm for the air and hydrogen, and a fuel cell temperature held at 65 °C. We also performed experiments at 80 °C in order to compare our results with the flow regime maps created by Hussaini and Wang [13]. The cell temperature was maintained with cartridge heaters in the endplates and a T-type thermocouple inserted into the anode endplate. The inlet gases were saturated with water vapor at the fuel cell temperature in both cases. Thus, approximately all of the water produced electrochemically is in the liquid state, which simplifies

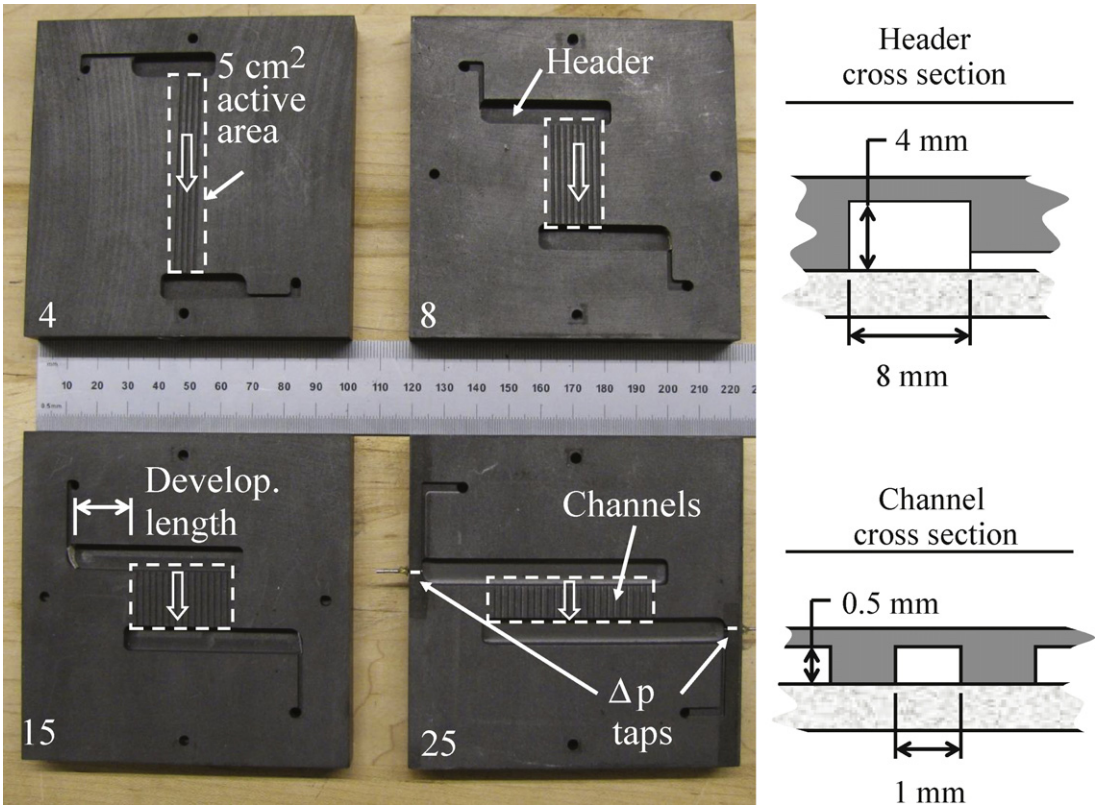

Fig. 2. Four cathode plates with 4, 8, 15, and 25 parallel channels. The plates have a constant active area of 5 cm^2 and the size of the header channels ensure that there is negligible pressure variation in the headers. During operation, the direction of gravity was aligned with the outlined arrows.

approximations of the superficial liquid velocity, u_l. An underlying assumption in calculating u_l in this way is that the amount of membrane water cross-over is negligible compared to the amount of water produced electrochemically. The assumption of zero membrane water cross-over is consistent with back diffusion balancing electro-osmotic drag and should not significantly change the general scaling relationships presented later. Membrane cross-over water typically results in <20% difference in water flow rate [15].

Pressure measurements were collected using a differential pressure transducer (Omega Engineering, Inc., Stamford, CT.), which had a full-scale range of 0–2.5 kPa. As Fig. 2 shows, the pressure difference was measured between the two headers. The pressure taps were formed by epoxing 1 mm diameter stainless steel tubes (Scanivalve, Liberty Lake, WA) into holes drilled through the side wall of the header channels. With the negligible pressure drop in the large diameter header channels, this pressure tap placement provides an accurate measurement point for the pressure drop across the microchannels.

In order to collect data at a range of different values of superficial gas velocities, experiments were conducted at a wide range of different air stoichiometric ratios (ranging from 1.1 to 40) with each of the four cathode flow field plates. For each experimental condition, the following procedural steps were followed after initial conditioning to establish repeatable results: (1) the hydrogen flow rate was set at a constant stoichiometric ratio of five based on the 5 cm^2 active area; (2) the air flow rate was set to the specific air stoichiometric ratio for the experiment and the fuel cell was allowed to equilibrate for 5 min with zero current in order to clear the channels of water from any previous experiments; (3) the current was set to 2 A for 5 min; and (4) the voltage data was collected for 30 min (10 data point per second). The high hydrogen flow rate was used to prevent any spurious anode influence on the results.

3. Results

3.1. Polarization curves

Fig. 3 presents polarization curves for the fuel cell with cathode plates having 8 and 25 channels at a constant air flow rate of 0.5 slpm (an air stoichiometric ratio of 5.5 at 1 A cm^{-2}). These polarization curves serve to illustrate the significant loss of performance when using a large number of channels in parallel. For example, the limiting current was 0.5 A cm^{-2} with 25 channels versus 1.9 A cm^{-2} with 8 channels. We also use the 8 channel polarization curve to demonstrate that the current–voltage characteristics of our masked MEAs are consistent with unaltered versions of the same commer-

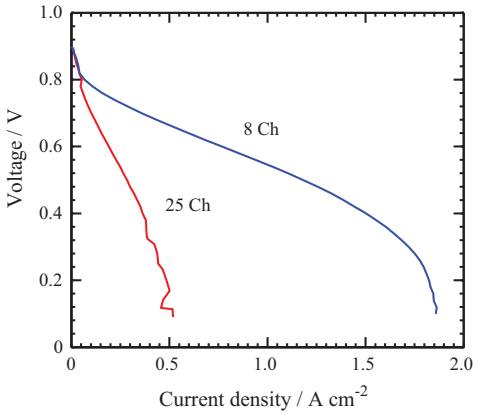

Fig. 3. Polarization curves for flow field plates with 8 and 25 channels. The fuel cell temperature was 65 °C and the air flow rate was 0.5 slpm. The scan rate of the polarization curves was 1 mV s^{-1}. The gases were fully humidified at the inlets.

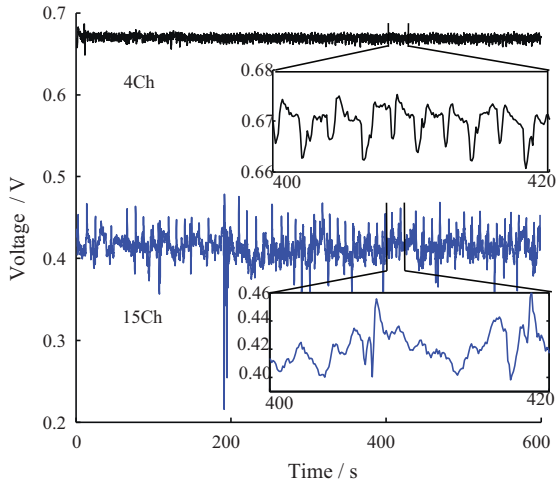

Fig. 4. Fuel cell voltage versus time for the cathode plates with 4 and 15 channels in parallel and an air stoichiometric ratio of 2. The current density was 0.4 A cm^{-2} and the cell temperature was 65 °C. The gases were fully humidified at the inlets.

cial MEA. From prior studies in the literature, a benchmark for the performance of this MEA and GDL combination at the same pressure (1 atm), humidification (100%), and temperature (within 10 °C of 65 °C) is a current density of approximately 0.8 A cm^{-2} at fuel cell voltage of 0.6 V when losses due to channel flooding are not present [16,17]. The current density of the 8 channel plate polarization curve was 0.77 A cm^{-2} at a voltage of 0.6 V, which is consistent with the benchmark.

3.2. Voltage time series

Fuel cell voltage data at a current density of 0.4 A cm^{-2} was collected for all four flow field configurations at two temperatures, 65 °C and 80 °C, and for varying values of the air stoichiometric ratio. Throughout the following results, the voltage behavior was studied at a constant current of 0.4 A cm^{-2} because it is well within the linear Ohmic region of the polarization curve and is far from the non-linear mass transport limited region in cases where channel flooding is not present. Thus, reductions in the effective active area and the commensurate increase in effective current density due to liquid water blocking channels and shutting down regions of the active area should have a approximately linear effect on the time-averaged voltage.

Fig. 4 shows representative fuel cell voltage time series for two different flow field geometries (4 and 15 parallel channels) at the same air stoichiometric ratio of 2 and an operating temperature of 65 °C. As expected, there was significantly lower average voltage with increased numbers of channels (greater channel plurality) due to liquid water accumulation in the channels. The increase in liquid water accumulation in the microchannels with larger numbers of channels, for a given volumetric rate of liquid water production, is due to a non-linear relationship between the liquid phase velocity and the air flow rate. Thus, greater water accumulation is commensurate with a larger liquid volume fraction (i.e., cross-sectional area) in the channels and lower velocities. In this particular case, the voltage was reduced by 37% when using 15 channels instead of 4 channels. The amplitude of the voltage fluctuation was also larger with greater numbers of channels, even though the air stoichiometric ratio and the current density were the same. As the inset plots in Fig. 4 illustrate, the typical fluctuations of the 15 channel case had an amplitude range roughly 4 times greater than that of the 4 channel case.

3.3. Correlation of pressure drop with voltage

To demonstrate that the voltage instabilities were primarily due to two-phase flow in the channels, we measured the pressure drop through the microchannels and evaluated the correlation between the voltage and pressure measurements. Fig. 5 shows voltage and pressure time series data collected at an air stoichiometric ratio of 1.5 in the 15 channel configuration. There are significant fluctuations in both pressure and voltage signals under these operating conditions. The figure also shows the power spectrum of the pressure and voltage time series. The power spectra have similar features at frequencies above 0.2 Hz; both feature a $1/f$ decrease in amplitude versus frequency and have peaks at the same frequencies. The correlation coefficient between the pressure and voltage was −0.41, and in a second set of data under the same conditions (not shown), the value was −0.40 for the correlation coefficient. This means that there was a significant negative correlation, meaning *increases* in pressure drop are moderately synchronized with *decreases* in fuel cell voltage. This is to be expected because an increase in pressure would indicate increased channel blockage and greater flow maldistribution, which result in regions of oxygen starvation.

3.4. Voltage power spectrum

We also constructed the power spectra of the voltage for all four plates in order to investigate the fluctuation in the frequency domain and evaluate the trends of dominant frequencies with changes in channel plurality and air stoichiometric ratio. Fig. 6 shows power spectrums of voltage fluctuations for the four flow field plates for air stoichiometric ratios ranging from 2 to 32. We observed the total amplitude of fluctuations decreased with increasing values of the air stoichiometric ratio as well as with decreasing numbers of channels. In general, the amplitude of the fluctuations decreased with increasing frequency with a $1/f$ dependence with several peaks occurring between 0.2 and 2.0 Hz. Peak frequencies with values on the same order of magnitude were measured by Chen [18] for the pressure drop time series in an *ex situ* two-channel apparatus and by Niroumand et al. [19] in an cathode flow channel of an operating fuel cell.

As Fig. 6 shows, there was a trend for peaks to shift to higher frequency values as the air stoichiometric ratio was increased with a fixed number of channels. Similarly, the peaks tended to shift to higher frequencies when using flow field plates with fewer channels. These trends in peak frequency are related to the change in velocity and residence time of the air in the microchannels as the flow rate was increased. Thus, these trends could be due to the fast removal of smaller droplets at higher air flow rates rather than the slow removal of larger droplet less often at lower air flow rates. This contrast is also evident in the voltage time series in Fig. 4. Two other important trends observed in the power spectrums are: (1) the disappearance of peaks with the highest stoichiometric ratios, which is consistent with using high gas velocities that prevent water accumulation, and (2) the diffusion of peaks into broad, high amplitude values with greater numbers of channels. This is particularly clear in the results for 25 channels. This entails that the two-phase flow disturbances are present across this entire range of frequencies because of the greater number of dynamic modes for flow field plates with greater numbers of channels.

3.5. Voltage loss scaling

We observed significant reductions in fuel cell voltage when using large numbers of channels in parallel. We define the voltage loss as the difference between the time-averaged, steady state voltage and that for the same plate at the highest air-stoichiometric

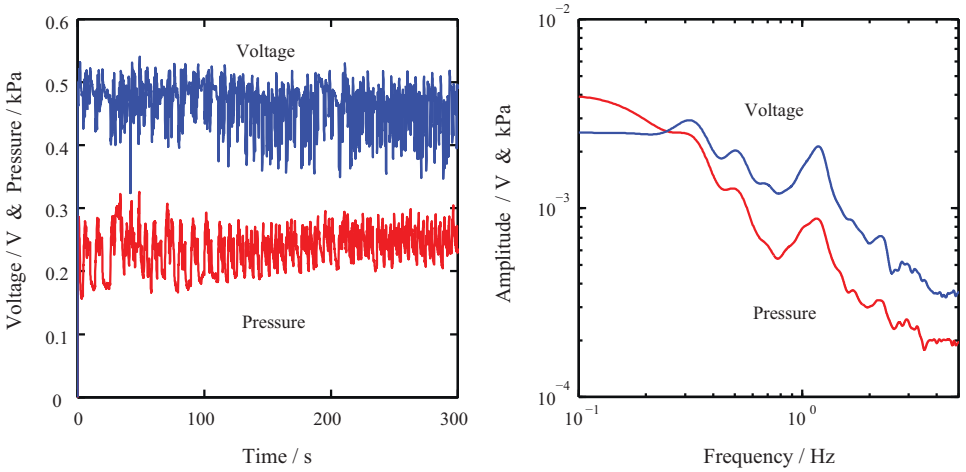

Fig. 5. Pressure and voltage time series (left) and power spectrums (right) for the 15 channel plate with an air stoichiometric ratio of 1.5. The fuel cell temperature was 65 °C and the current density was 0.4 A cm^{-2}. The gases were fully humidified at the inlets.

ratio tested. For example, the time-averaged voltage with the 25 channel plate at 80 °C decreased 0.17 V when the air stoichiometric ratio was reduced from 40 to 3. Herein, we evaluate the scaling of the voltage loss normalized by time-averaged voltage at the highest stoichiometric ratio. For example, the 0.17 V voltage loss with the reduction of the stoichiometric ratio from 40 to 3 is equivalent to a normalized voltage loss of 0.26 given the time-averaged fuel cell voltage was 0.65 V at the highest stoichiometric value of 40.

Power series curves were fit through each of the data sets and the two free variables in the power curve fits were used to estimate the dependencies on the number of channels, N, and the air stoichiometric ratio, ζ. Rounded to the nearest half-integer, the normalized voltage loss data scaled linearly with the number of channels, N, and inversely with the air flow stoichiometric ratio, ζ. Fig. 7 plots the normalized voltage loss versus N/ζ and illustrates a diffuse collapse of the data with this scaling. The R^2 correlation coefficient of the power fit through the voltage loss was 0.70. The equation for normalized voltage loss power series fit is $(\bar{V}_{max} - \bar{V})/\bar{V}_{max} = 0.032N/\zeta$. The scaling shows that each time the number of channels (or channel plurality) is doubled, the voltage loss due to flooding roughly doubles for a constant stoichiometric ratio and current density. The scaling also shows that each time the air flow rate is doubled, the voltage loss is approximately halved, for a constant electrochemical area and current density. We note that, on average, there was slightly more voltage loss when operating at 65 °C.

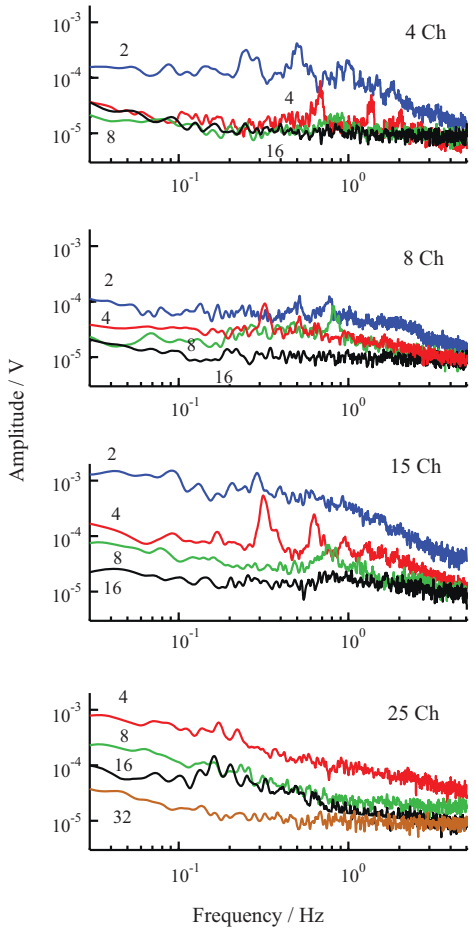

Fig. 6. Power spectrum of voltage fluctuations with varying air stoichiometric ratios and number of microchannels in the cathode plate. The fuel cell temperature was 65 °C and the current density was 0.4 A cm^{-2}. Note that it was not possible to operate with 25 channels and an air stoichiometric ratio of 2 due to severe flooding of the microchannels. The gases were fully humidified at the inlets.

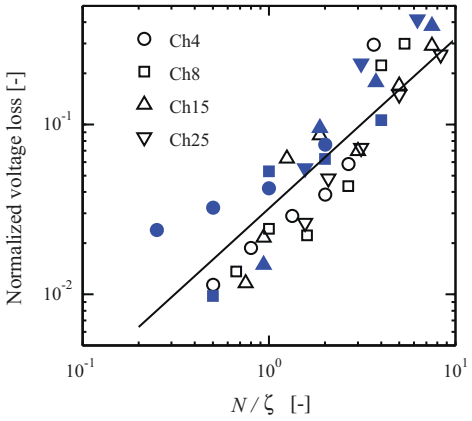

Fig. 7. Normalized voltage loss versus the number of channels divided by the air stoichiometric ratio, N/ζ. The open symbols are data collected at a fuel cell temperature of 80 °C and the filled symbols are data for 65 °C. For all channel configurations and temperatures, the current density was 0.4 A cm^{-2}. The gases were fully humidified at the inlets.

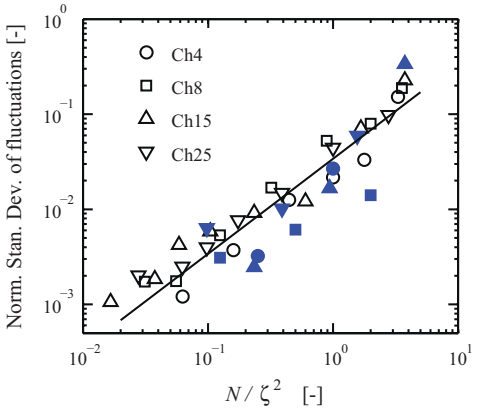

Fig. 8. Standard deviation of the voltage normalized by the time-averaged voltage versus the number of channels divided by the air flow stoichiometric ratio squared, N/ζ^2. The open symbols are data collected at 80 °C, and the filled symbols are data collected at 65 °C. For all channel configurations and temperatures, the current density was 0.4 A cm^{-2}. The gases were fully humidified at the inlets.

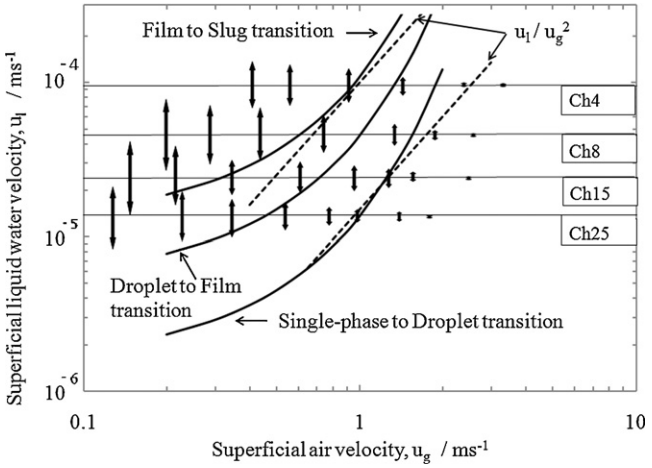

Fig. 9. Voltage fluctuation versus flow regime compared with flow transitions as observed by Hussaini and Wang [13] under similar microchannel geometry, pressure, and temperature. The vertical height of the arrow represents the amplitude of the voltage fluctuation (80 °C data) in a $\log_{10}$ scale. Solid curves are their fits for the transitions between flow regimes. The dashed curves are guide-lines showing our u_l/u_g^2 scaling for voltage fluctuations.

3.6. Voltage fluctuation scaling

In this work we have quantified the voltage fluctuation amplitude as the standard deviation of the voltage time-series normalized by the time-averaged voltage of the same time series. As Fig. 4 illustrated, using greater numbers of channels in parallel can dramatically increase the amplitude of the voltage fluctuations. Rounded to the nearest half-integer, the voltage fluctuation data scaled linearly with the number of channels, N, and inversely with the square of the air stoichiometric ratio, ζ. Fig. 8 plots the normalized standard deviation of the voltage versus N/ζ^2 and shows a tight collapse of the data with this scaling. The R^2 correlation coefficient of the power fit through the voltage fluctuation data was 0.87. The equation for normalized voltage standard deviation power series fit is $\bar{\sigma}_V/\bar{V} = 0.034N/\zeta^2$. For voltage fluctuations, the air stoichiometric ratio has a leading order effect with its inverse quadratic scaling. As an example, the voltage standard deviation is reduced to roughly a quarter of its previous value if the air stoichiometric ratio is doubled. In addition, the number of channels (channel plurality) has a proportional effect. According to this scaling, doubling the number of channels (doubling channel plurality) results in a doubling of the normalized voltage standard deviation.

4. Discussion

In order to compare our results with prior studies on two-phase flow in the microchannels of PEM fuel cells, the parameters in this report were converted to the following flow regime variables: superficial liquid velocity, u_l, and superficial air flow velocity, u_g. Since the water produced was roughly constant in all of the data points (due to the constant current and fully humidified conditions), u_l is only a function of N: $u_l \propto 1/N$. The superficial air velocity was a function of both the air stoichiometric ratio and the number of channels:

$$u_g \propto \frac{\zeta}{N}.$$

Therefore, the N/ζ^2 dependence of the voltage fluctuations suggests that the fluctuations scale as u_l/u_g^2. The mean voltage loss scaled as N/ζ, and hence as u_g^{-1}. However, we are not suggesting that there is no dependence on u_l, but that it is a significantly weaker parameter than u_g, in determining the voltage loss.

We use the u_g and u_l conversion to compare our voltage fluctuation amplitude data and scaling with the results from Hussaini and Wang [13] under similar geometric and operating conditions. They observed the flow regimes in cathode microchannels with 0.5 mm by 1 mm cross-sections at 1 atm and 80 °C, which is the same operating conditions as the 80 °C data presented in Fig. 8. Their 14 cm^2 cathode flow field had seven channels, resulting in a channel plurality value of 0.5 cm^{-2}. Fig. 9 shows the voltage fluctuation amplitude data collected in this work overlaid against their flow map. The height of the vertical arrows represents the amplitude of the voltage fluctuation in a $\log_{10}$ scale. The solid curves in Fig. 9 are their fits for the transitions between the single phase, droplet, film, and slug flow regimes. The amplitude of the pressure fluctuation measured by Lu et al. [10] follow the same trend for the amplitude of the pressure fluctuations: slug > film > mist. The dashed curves in Fig. 9 show the slope of our u_l/u_g^2 scaling for the voltage fluctuation amplitude. Note that the u_l/u_g^2 scaling roughly matches the slope of lines defining the flow regime transitions measured by Hussaini and Wang [13] over a large portion of their flow map. The amplitude of our measured voltage fluctuations was largest in flow regime map region where Hussaini and Wang [13] observed slug flow. As expected, our fluctuation amplitude decreased as our superficial velocities enter the film, mist, and single-phase flow regions within their flow regime map.

4.1. Generalization

We now discuss generalizing our findings to fuel cells of varying active area and channel cross-sectional dimensions. We base this generalization on the flow regime's dependence on the parameters u_g and u_l for a given flow field design. For example, flow regime maps, such as that shown in Fig. 9, attempt to uniquely define the flow regime based on these two parameters. For a flow field of arbitrary channel numbers and channel cross-sectional dimensions with 100% inlet relative humidity, the expressions for the superficial gas and liquid velocities are:

$$u_g = C_g \frac{i\zeta}{\chi A_c} \quad (1)$$

and

$$u_l = C_l \frac{i}{\chi A_c} \quad (2)$$

where i is the current density, A_c is the cross-sectional area of each channel, and C_g and C_l are constants relating the current to

the stoichiometric volumetric flow rate. When considering, similar operating conditions (e.g., current density), the scaling of the velocities reduce to:

$$u_g \propto \frac{\zeta}{\chi A_c} \propto \frac{\zeta}{\chi^*} \tag{3}$$

and

$$u_l \propto \frac{1}{\chi A_c} \propto \frac{1}{\chi^*} \tag{4}$$

where χ^* is the dimensionless channel plurality, $\chi^* = \chi A_c$, which is also the ratio of the total channel cross-sectional area to the active area, $\chi^* = NA_c/A$.

The voltage loss and fluctuation amplitude results showed a proportional dependence on the number of channels, which is equivalent to channel plurality since our study was done with constant active area. Thus, we suggest substituting the expression for dimensionless channel plurality into the equation fits for the normalized voltage loss (see Section 3.5):

$$\frac{\bar{V}_{\max} - \bar{V}}{\bar{V}_{\max}} = 32\frac{\chi^*}{\zeta} \tag{5}$$

and the voltage fluctuation amplitude (see Section 3.6):

$$\frac{\bar{\sigma}_V}{\bar{V}} = 34\frac{\chi^*}{\zeta^2} \tag{6}$$

The valid parameter ranges for the voltage loss and voltage fluctuation amplitude scaling are $2 \times 10^{-4} < \chi^*/\zeta < 8.5 \times 10^{-3}$ and $1.5 \times 10^{-5} < \chi^*/\zeta^2 < 3 \times 10^{-3}$, respectively. A typical χ^*/ζ value from a recent study by industry is 7×10^{-4} [14], which falls well within the range of values studied here. It is important to note that the constants of 32 and 34 in Eqs. (5) and (6) were obtained for our particular channel cross-sectional dimensions. Thus, care should be taken when using the χ^* to generalize our findings to flow fields with significantly different hydraulic diameters. In our future work, we will extend our studies of channel plurality to include channels of varying cross-sectional dimensions and other active areas to further verify the χ^* scaling.

5. Conclusion

The PEM fuel cell voltage loss and fluctuations measured in this study are caused by two-phase flow instabilities in the microchannels of the cathode. Since the air velocity distribution and liquid accumulation in the microchannels vary in time with these instabilities, the rate of oxygen transport to the cathode catalyst layer is reduced and fluctuates in time, causing the voltage to fluctuate and an overall decrease in the mean voltage. In this study, we investigated the effect of channel plurality on the fuel cell voltage using a custom set of plates with varying numbers of microchannels. We showed that the cause of the voltage fluctuations was the fluctuations in the liquid flooding of the microchannels by (a) measuring a negative correlation coefficient (−0.4) between the pressure and voltage in the case of large amplitude fluctuations and (b) comparing our data with the flow regime data collected by Hussaini and Wang [13]. Through a large experimental parametric study, we found that the voltage loss scales proportionally with channel plurality divided by the air stoichiometric ratio. We also identified that the amplitude of the voltage fluctuations scaled proportionally to the channel plurality divided by the air stoichiometric ratio squared. Knowing these general scalings for the voltage loss and fluctuation amplitude may be of considerable value in the design of commercial PEM fuel cells and in the validation of two-phase models for the flow in the microchannels.

Acknowledgements

We thank Chi-Shin Ho and Colin O'Shea for the construction of the cathode flow channel plates. We also thank Carnegie Mellon University's Berkman Faculty Development Fund for the support of this research.

References

[1] T. Klaiber, Automotive power units with pem fuel-cells, Chem-Ing-Tech 67 (1995) 1292–1299.
[2] R.K. Ahluwalia, X.H. Wang, Fuel cell systems for transportation: status and trends, J. Power Sources 177 (2008) 167–176.
[3] R. Anderson, L.F. Zhang, Y.L. Ding, M. Blanco, X.T. Bi, D.P. Wilkinson, A critical review of two-phase flow in gas flow channels of proton exchange membrane fuel cells, J. Power Sources 195 (2010) 4531–4553.
[4] H. Li, Y.H. Tang, Z.W. Wang, Z. Shi, S.H. Wu, D.T. Song, J.L. Zhang, K. Fatih, J.J. Zhang, H.J. Wang, Z.S. Liu, R. Abouatallah, A. Mazza, A review of water flooding issues in the proton exchange membrane fuel cell, J. Power Sources 178 (2008) 103–117.
[5] G. Minor, X. Zhu, P. Oshkai, P. Sui, N. Djilali, Mini-Micro Fuel Cells, Springer Books, 2008, ISBN 1874-6519, pp. 153–170.
[6] J.X. Chen, Experimental study on the two phase flow behavior in PEM fuel cell parallel channels with porous media inserts, J. Power Sources 195 (2010) 1122–1129.
[7] J. Dillet, O. Lottin, G. Maranzana, S. Didierjean, D. Conteau, C. Bonnet, Direct observation of the two-phase flow in the air channel of a proton exchange membrane fuel cell and of the effects of a clogging/unclogging sequence on the current density distribution, J. Power Sources 195 (2010) 2795–2799.
[8] G. Karimi, F. Jafarpour, X. Li, Characterization of flooding and two-phase flow in polymer electrolyte membrane fuel cell stacks, J. Power Sources 187 (2009) 156–164.
[9] E.C. Kumbur, K.V. Sharp, M.M. Mench, Liquid droplet behavior and instability in a polymer electrolyte fuel cell flow channel, J. Power Sources 161 (2006) 333–345.
[10] Z. Lu, S.G. Kandlikar, C. Rath, M. Grimm, W. Domigan, A.D. White, M. Hardbarger, J.P. Owejan, T.A. Trabold, Water management studies in PEM fuel cells, Part II: ex situ investigation of flow maldistribution, pressure drop and two-phase flow pattern in gas channels, Int. J. Hydrogen Energy 34 (2009) 3445–3456.
[11] A. Theodorakakos, T. Ous, A. Gavaises, J.M. Nouri, N. Nikolopoulos, H. Yanagihara, Dynamics of water droplets detached from porous surfaces of relevance to PEM fuel cells, J. Colloid Interface Sci. 300 (2006) 673–687.
[12] L.F. Zhang, H.T. Bi, D.P. Wilkinson, J. Stumper, H.J. Wang, Gas-liquid two-phase flow patterns in parallel channels for fuel cells, J. Power Sources 183 (2008) 643–650.
[13] I.S. Hussaini, C.Y. Wang, Visualization and quantification of cathode channel flooding in PEM fuel cells, J. Power Sources 187 (2009) 444–451.
[14] J.P. Owejan, J.J. Gagliardo, S.R. Falta, T.A. Trabold, Accumulation, Removal of liquid water in proton exchange membrane fuel cells, J. Electrochem. Soc. 156 (2009) B1475–B1483.
[15] G.J.M. Janssen, M.L.J. Overvelde, Water transport in the proton-exchange membrane fuel cell: measurements of the effective drag coefficient, J. Power Sources 101 (2001) 117–125.
[16] K. Karan, H. Atiyeh, A. Phoenix, E. Halliop, J. Pharoah, B. Peppley, An experimental investigation of water transport in PEMFCs, Electrochem. Solid-State Lett. 10 (2007) B34–B38.
[17] S. Litster, C.R. Buie, T. Fabian, J.K. Eaton, J.G. Santiago, Active water management for PEM fuel cells, J. Electrochem. Soc. 154 (2007) B1049–B1058.
[18] J.X. Chen, Dominant frequency of pressure drop signal as a novel diagnostic tool for the water removal in proton exchange membrane fuel cell flow channel, J. Power Sources 195 (2010) 1177–1181.
[19] A.M. Niroumand, W. Merida, M. Eikerling, M. Saif, Pressure–voltage oscillations as a diagnostic tool for PEFC cathodes, Electrochem. Commun. 12 (2010) 122–124.